Academic Journal of Science and Technology
ISSN: 2771-3032 | Vol. 18, No. 3, 2025

Lightweight Design of Composite Battery Case Upper Cover Based on NSGA-II Algorithm

Jianqiao Li [a], Yan Peng *

School of Mechanical Engineering, Sichuan University of Science & Engineering, Yibin Sichuan, 644600, China
*** Corresponding author:** Yan Peng (Email: 2634932795@qq.com), [a] 1984525334@qq.com

Abstract: In response to the lightweight demand for battery packs of new energy vehicles and the development of composite flame-retardant technology, this paper proposes a multi-objective optimization method for composite upper covers based on the NSGA-II algorithm. Firstly, the mechanical properties of aluminum alloy materials and two types of composite materials are compared. Then, a battery pack model is established and preprocessed, and the thickness of the composite upper cover is calculated according to the equal stiffness approximation theory. Subsequently, the partitioned thickness of the upper cover is set as a variable to determine the optimization objectives, and the optimal Latin hypercube design method is used to generate sample points. By comparing the accuracy of three surrogate models, namely Response Surface Methodology (RSM), Kriging, and Radial Basis Function (RBF), the RSM surrogate model is selected as the optimal one. Furthermore, the RSM model is substituted into the NSGA-II algorithm to solve the multi-objective optimization model, and finally the optimal scheme for the thickness of the composite upper cover is obtained. The optimization results show that within the range of modal error less than 0.1Hz, the mass of the structural part is reduced by 1.99kg, representing a 15% mass reduction. This demonstrates the lightweight effect and feasibility of the method, and verifies the application potential of the composite material in the field of battery cases.

Keywords: Finite Element Analysis; Surrogate Model; Lightweight; Multi-Objective Optimization; NSGA-II Algorithm; Battery Pack Upper Cover.

1. Preface

Lightweighting mainly comes from two ways, one is the structural optimization design, the other is the application of high strength and lightweight materials. Carbon fiber composite materials are widely used in aerospace, aviation and automobile industry because of their high strength, high toughness, high plasticity and impact resistance.[1].

CF/PA66 (carbon fiber-reinforced nylon 66) composites have gained significant attention for their lightweight, high strength, and exceptional corrosion and wear resistance. As a thermoplastic composite, they demonstrate superior impact resistance and energy absorption capabilities compared to the brittle thermosetting resins, which is crucial in scenarios like vehicle collisions. [2] The molding process involves physical melting and cooling. Compared to the chemical curing reaction of thermosetting resins, it offers significant advantages such as high production efficiency and short molding cycle.[3]Moreover, the eco-friendly and recyclable nature of thermoplastic composites aligns with sustainable development requirements.[4]In terms of mechanical properties, CF/PA66 fully meets the stringent requirements for structural rigidity and strength in battery cases. [5] However, GB38031-2025[6] Article 5.2.7 of the "Safety Requirements for Power Batteries in Electric Vehicles" stipulates that battery systems must prevent flame spread within two hours after thermal runaway, imposing stricter requirements on the flame retardancy of battery case materials. Non-metallic materials must meet UL 94V0 flame retardancy standards, as PA66s flame retardancy rating (e.g., UL 94HB) fails to satisfy safety standards for electric vehicles. Furthermore, the composition and toxicity of gases produced during combustion are critical safety indicators, directly impacting the lives of drivers and passengers. [7] Therefore, flame-retardant modification of the base CF/PA66 material and systematic evaluation of its combustion toxicity and smoke density are critical challenges in battery case applications. As demonstrated by Markforged [8] The companys OnyxFR is a composite material filled with nylon and chopped carbon fiber. With a thickness of 3mm, it achieves the V-0 rating in the UL94 flame test. Provided that mechanical properties are met, a 3mm thickness is acceptable for battery enclosures. Qu Rihua et al. [9] Thermal gravimetric analysis of the composite material shows that carbon fibers exhibit excellent thermal stability. As the carbon fiber content increases, the materials thermal stability progressively improves, indicating enhanced flame retardancy. Chen Xiaokai [10] Researchers proposed a lightweight design methodology for multi-material power battery enclosures in electric vehicles. Through sensitivity analysis, they quantified each components contribution to optimizing both weight and first-order natural frequency. The resulting CFRP-aluminum alloy composite structure achieved a 48.86% weight reduction while boosting the first-order natural frequency to 32.03Hz. The study also explored replacing metal components with carbon fiber composites. Ma Qi-hua [11] By applying the equivalent stiffness principle, the cross-sectional performance of the composite battery pack was determined. Manufacturing validation was conducted for different lamination methods, while the lower housing underwent three optimization phases: free-form sizing, dimensional optimization, and lamination sequence optimization to achieve the lightest structure. The upper housing was reinforced with a distinctive "Wang" character-shaped design. The final battery pack achieved a total weight of 14.09kg, representing a 56% weight reduction. With continuous advancements in composite material flame retardancy technology, more material options now exist, enabling further lightweight optimization of battery cases. Future technological breakthroughs are expected to expand

the application of composite materials in this field. This study innovatively selected composite material battery case lids based on the implementation of new national standards and improved flame retardancy technologies, demonstrating the feasibility of lightweight solutions.

2. Upper Cover Composite Material Comparison

To meet battery case operational requirements and modal standards, this study evaluated three lightweight materials for the battery case lid: glass fiber-reinforced polypropylene (30% GF/PP), chopped carbon fiber-reinforced nylon (30% CF/PA66), and carbon fiber reinforced plastic (CFRP). The 30% CF/PA66 configuration was ultimately selected as the optimal solution.

Table 1. Material Parameters

performance index	30%GF/PP	30%CF/PA66	CFRP
Tensile modulus (GPa)	9.5	16.1	70-140
Shear modulus (GPa)	3.2	5.8	4.5-7.0
Interlayer strength (MPa)	40	55	25-35
Density (kg/m³)	1200	1260	1550

From a density perspective, all three materials demonstrate potential for lightweight applications. However, CFRPs inherent anisotropy makes it challenging to function independently in structural components, leading to modal splitting. Simulation results indicate excessively high modal frequencies (first-order 82.4Hz/ second-order 94.7Hz), where higher-order modes overlap with high-frequency motor frequencies, causing high-frequency vibration coupling. Additionally, CFRP manufacturing costs are significantly higher than the other two materials. Therefore, it is more suitable to integrate CFRP with steel through optimized layering configurations in structural designs.

The performance gap between 30% GF/PP and raw aluminum alloy is substantial, and neither equivalent stiffness replacement nor simulation modeling can achieve lightweight objectives. This study therefore selects 30% chopped carbon fiber-reinforced nylon PA66 composite, which uniformly disperses high-strength, high-modulus chopped carbon fibers into the PA66 matrix. This configuration avoids directional anisotropy caused by fiber orientation and forms a high-performance material through interfacial bonding. PA66, a commonly used engineering plastic, inherently possesses excellent wear resistance, self-lubrication properties, and mechanical strength. Carbon fibers, renowned for their lightweight, high strength, and rigidity, create significant synergistic effects when combined with PA66.

Among various carbon fiber content ratios, PA66 reinforced with 30% carbon fiber demonstrates unique balance advantages. When the carbon fiber content is too low, the materials reinforcement effect becomes negligible; conversely, excessive content leads to a significant increase in melt viscosity, which not only complicates processing but may also degrade material properties due to carbon fiber agglomeration. The 30% carbon fiber content fully leverages the reinforcing effects of carbon fibers.[12]It is expected that the injection molding cycle will be shortened by 50%, the risk of welding deformation will be eliminated, and the integrated sealing structure (eliminating the separate sealing strip) can ensure the comprehensive performance of the material, and the comprehensive cost is lower than that of aluminum alloy, which is an ideal choice to balance the performance improvement and cost control.

3. Cover Performance Analysis

3.1. Finite Element Model

The battery box cover primarily serves as a sealing and isolation component for power batteries. According to the national standard GB38031-2025, compliance is evaluated through two aspects: simulated operating conditions and modal analysis. With mature material applications and optimized structural designs, current battery box deformation control in simulated conditions has significantly exceeded standard requirements. The critical considerations are ensuring lower-order modal frequencies surpass road excitation levels while preventing high-order modal overlaps with high-frequency motor vibrations. This study focuses on modal optimization. As the paper analyzes the lightweight effects of replacing conventional aluminum alloy materials with composite materials and optimizing the battery box cover, targeted modal and operational condition analyses are conducted to save finite element analysis time. For subsequent simulation experiments, a geometrically simplified model is established with precision assurance through battery pack development case studies.

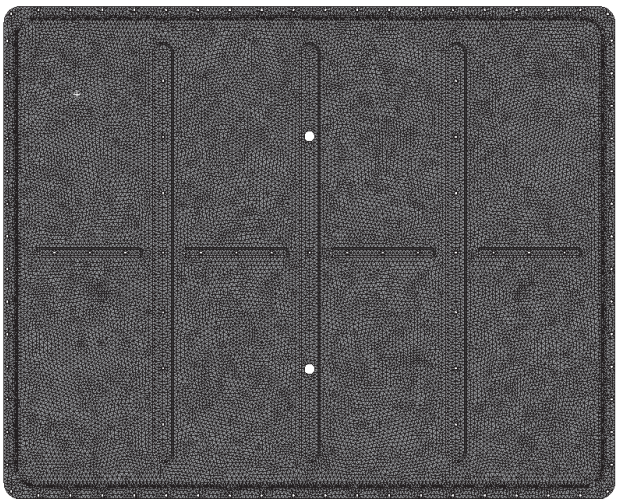


Figure 1. Upper cover finite element model

Using ANSYS software, the covers geometric model is simplified and preprocessed with meshing. Minor features like chamfers and fillets are simplified while maintaining computational accuracy. Boundary conditions fix installation

bolt holes, with mesh elements sized at 10mm and mass 0.8≥0.5 meeting standards. The final mesh comprises 343,494 nodes and 169,465 elements, as shown in the figure 1.

The battery box cover is initially made of 6061-T6 aluminum alloy, a heat-treated high-performance alloy that combines lightweight characteristics with structural strength. This corrosion-resistant material features excellent weldability, machinability, and low density, making it widely used in industrial, transportation, and aerospace applications. As a result, the aluminum alloy cover weighs only 13.224kg. The material properties are detailed in the table below.

Table 2. Aluminum Alloy Parameters

material	thickness /mm	modulus of elasticity /GPa	Poisson ratio	Density (kg/m3)
6061-T6	2	68.9	0.33	2750

3.2. Stiffness Substitution Method

In lightweight design with material substitution, the equivalent stiffness approximation theory is typically employed to select new materials for weight reduction. [13]

Stiffness replacement refers to the adjustment of parameters to maintain the stiffness (EI) of the components before and after replacement when the material is replaced or the section form is changed, so as to ensure that the deformation characteristics of the structure remain unchanged.

The basic expression of the stiffness of a member. For linear elastic materials, the stiffness formula is:

$$K = EI$$

E: Elastic modulus of the material (which reflects its resistance to elastic deformation). I: Inertial moment of the cross-section (which reflects the cross-sections ability to resist bending deformation).

$$E_M I_M = E_C I_C$$

$$E_M \frac{b_M h_M^3}{12} = E_C \frac{b_C h_C^3}{12}$$

In the formula, EM and IM represent the elastic modulus and the cross-sectional moment of inertia of the original structure, respectively; EC denotes the equivalent modulus of the laminated composite; IC is the moment of inertia of the composite structures cross-section; b stands for the width, and h indicates the thickness of the cross-section. By applying the above formula, the thickness ratio of the equivalent stiffness material before and after replacement can be derived:

$$\frac{t_M}{t_C} = \left(\frac{E_C}{E_M}\right)^{\frac{1}{\theta}}$$

Among them, α is the thickness index coefficient. According to practical engineering experience, for automotive parts, its value is usually between 1 and 3. The larger the value of α, the more obvious the lightweight effect. In this paper, the thickness index coefficient α=2 value is in line with automotive parts engineering practice.[14]

TC and TM represent the cross-sectional thickness of the carbon fiber composite structure after replacement and the original metal structure, respectively. Calculations show that replacing 2mm of aluminum alloy with composite material yields a rounded value of 4mm.

3.3. Condition Performance Analysis

The battery pack box body after equivalent stiffness replacement is preliminarily simulated and analyzed to obtain the simulation results under various working conditions.

3.3.1. Static Strength Simulation Analysis

The battery pack structure in vehicles faces multiple complex operating conditions during operation. To ensure optimal performance and reliability, vibration and static conditions must be considered during design. Static conditions require consideration of potential combinations of extreme scenarios. The standard specifies that under 1g, structural deformation should not exceed 1mm; under 3g, deformation should not exceed 3mm. [15] To simulate extreme road conditions, three scenarios were designed: bumpy road, sharp turns on bumpy road, and sudden braking on bumpy road. The loading methods for each scenario are shown in the table.

Table 3. Operating Conditions

operating mode	X axle	Y axle	Z axle
Bumpy road	--	--	4g
Sharp turn on bumpy road	1g	--	3g
Sudden braking on bumpy road	--	1g	3g

(1) The simulation results of the strength of aluminum alloy are shown in the figure:

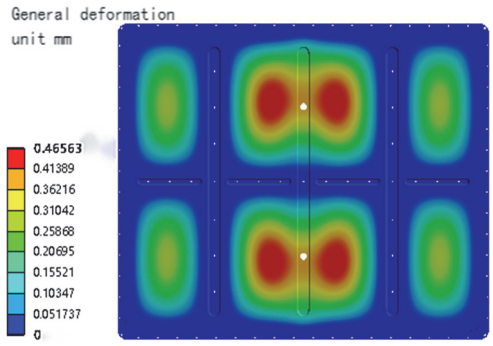


Figure 2. Static strength simulation of bumpy road

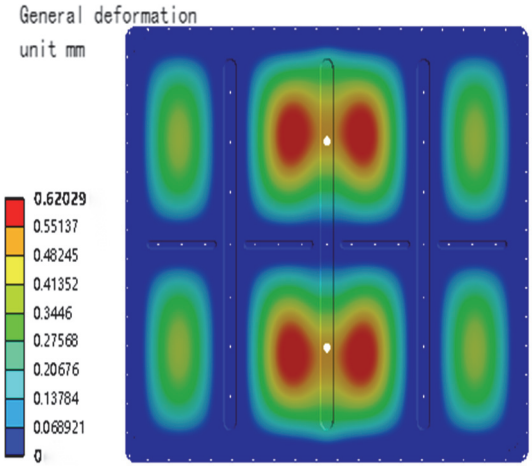


Figure 3. Static strength simulation of sharp turn on bumpy road

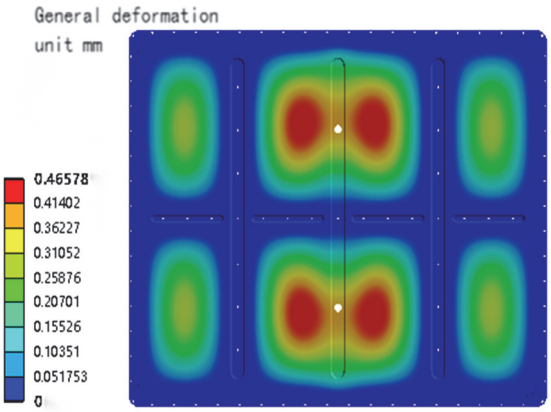


Figure 4. Static strength simulation of emergency braking on bumpy road

(2) The 30PA66 static strength simulation results are shown in the figure:

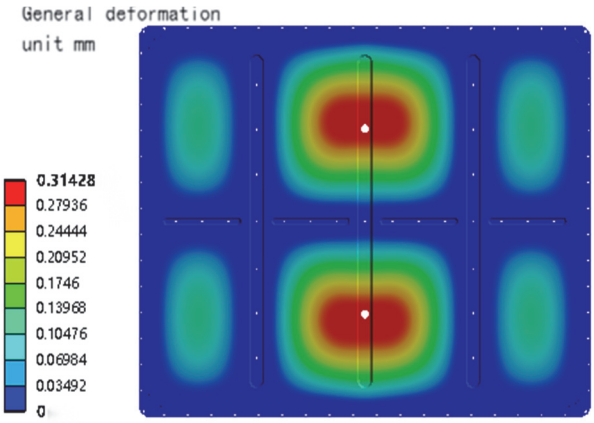


Figure 5. Static strength simulation of bumpy road

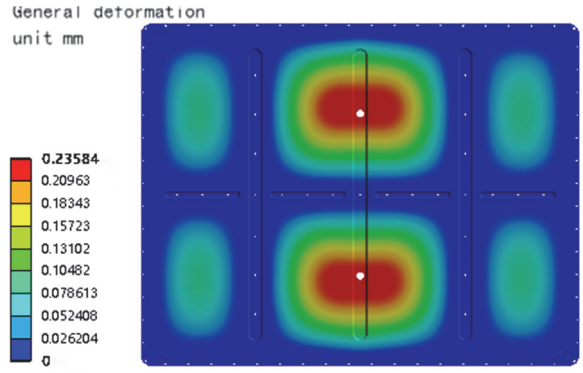


Figure 6. Static strength simulation of sharp turn on bumpy road

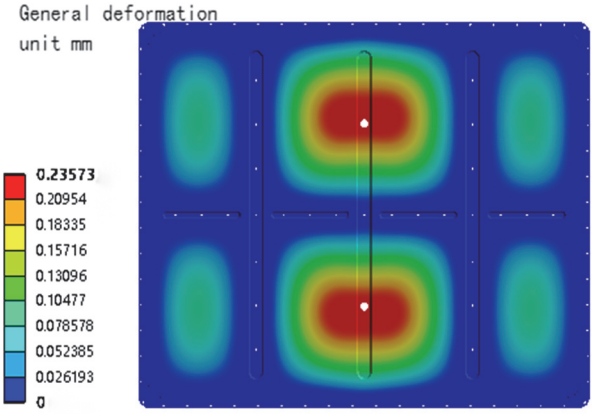


Figure 7. Static strength simulation of emergency braking on bumpy road

According to the simulation results above, the obtained performance comparison under working conditions is shown in the table.

Table 4. Comparison of static condition simulation

operating mode	alufer	Carbon fiber nylon
Bumpy road	0.62mm	0.31mm
Sharp turn on bumpy road	0.47mm	0.24mm
Sudden braking on bumpy road	0.47mm	0.24mm

3.3.2. Modal Analysis

Vibration operating conditions must not induce resonance with other automotive structural components, as this could cause structural damage. Modal analysis essentially involves theoretical modeling to establish mathematical models for system eigenvalue problems, solving which requires various approximation methods to determine system eigenvalues and eigenvectors. Typically, passenger vehicle chassis vibrations predominantly occur in the 50-100Hz range (e.g., idle 5-30Hz, road bumps 30-80Hz). The first-order mode should be ≥50Hz (to avoid the 30-50Hz chassis resonance zone) and ≤150Hz (to prevent overlap with motor high-frequency vibrations). Design considerations must account for various excitation influences, so the first-order mode is generally designed to exceed 30Hz. [16] In actual products, the modal frequency is affected by safety margins for accidental and prolonged attenuation, so the actual standard is set above 30Hz to enhance product stability. The modal simulation results of the two materials are shown in the table below.

Table 5. Modal Simulation Comparison

modality /Hz	alufer	Carbon fiber nylon
first order	63.50	64.98
second order	67.81	68.42
tervalence	75.44	94.95
4th order	77.41	96.37
5th order	85.51	112.74
Sixth order	85.54	112.84

A preliminary comparison of the composite battery pack cover with the same stiffness replacement with the aluminum alloy battery pack cover is shown below, and the static strength and modal simulation analysis of the two are as follows:

In static load conditions, aluminum alloy exhibits maximum deformation at both sides of the central section. Under Z-axis 4g load conditions on a bumpy road surface, aluminum alloy demonstrates a maximum displacement of 0.62mm, while composite material shows 0.314mm displacement under the same conditions. The maximum deformation of composite material remains lower than that of aluminum alloy. Under the other two static load conditions, composite material also demonstrates a slight advantage over aluminum alloy, with both materials showing significantly better performance than the standard requirements: deformation under 1g load should be less than 1mm, and under 3g load should be less than 3mm. This clearly indicates that both aluminum alloy and 30% CF/PA66 are high-performance materials for roof cover applications.

In modal simulation, the first-order constrained mode of

composite material is 64.97Hz, which shows a slight improvement compared to the original aluminum alloys first-order mode (63.49Hz), with both exceeding the standard frequency of 50Hz. The sixth-order constrained modes are 112.84Hz for composite material and 85.53Hz for aluminum alloy, both kept below 150Hz to avoid overlapping with high-frequency motor frequencies. In practical production, sufficient safety margins are reserved to account for material and connection attenuation under prolonged and complex environmental conditions. Mature products typically feature modal frequencies above 50Hz to enhance stability.

The aluminum alloy material cover weighs 13.201kg, while the composite material cover weighs 11.984kg. As both are excellent lightweight materials, replacing the equivalent stiffness material achieves a 1.217kg weight reduction with nearly unchanged or slightly improved performance, demonstrating a 9.2% weight reduction. Compared to the aluminum alloy material that balances strength and weight reduction, this proves effective lightweight optimization. However, the improvements are still preliminary and theres room for further enhancement.

4. Construction and Solution of Multi-Objective Optimization Model

4.1. Design Variable Selection

Given that this model represents only the upper cover component of a mature product and the battery pack integrates multiple systems, the overall design involves complex interactions among electrical systems. To achieve multi-objective optimization while maintaining critical connection and contact structures, this study selects three design variables: thickness of three regions in the battery box cover for lightweight composite material optimization. The cover body, connecting edge, and ribbed area correspond to variables x1, x2, and x3 respectively. Since variables x2 and x3 participate in bolted connections with the housing, they should not be excessively thin. Additionally, the material must achieve UL94V-0 flame retardancy rating at 3mm thickness. Considering typical ±20% tolerance ranges, the design variables are set with upper limits of 5mm and lower limits of 3mm, as shown in the table.

Table 6. Variable Design Range

design variable	x1	x2	x3
Initial thickness/mm	4	4	4
superior limit	5	5	5
lower limit	3	3	3

In multi-objective optimization, the design of each regional thickness is based on the premise that the performance of the upper cover is close to that of the aluminum alloy material, and the reduction of mass is compared to reflect the advantage of lightweight composite material.

The response objectives are the core metrics for subsequent optimization, including: the first-order modal frequency (Hz) of the aluminum alloy model, with the constraint that the difference between the final modal value and the aluminum alloy models modal frequency should be ≤0.5Hz; and the structural mass (kg) should be minimized.

The following is the definition of the multi-objective optimization problem.

Optimization Objective 1 (Modal Matching):

$$\min\left|f_{opt} - f_{Al}\right|$$

among

f_{Opt} represents the first−order modal frequency (Hz) of the optimized structure. f_{Al} denotes the first−order modal frequency (Hz) of the aluminum alloy structure.

Optimization Goal 2 (Lightweight):

$$\Delta m = \left(m_{raw} - m_{opt}\right)/m_{raw} \times 100\%$$

among m_{Opt} represents the optimized structures mass (kg). m_{Raw} represents the structural mass prior to optimization (kg).

constraint condition: $\left|f_{opt} - f_{Al}\right| \leq 0.1\text{Hz}$

This constraint ensures that the first-order modal frequency of the optimized structure deviates from that of the aluminum alloy structure by no more than 0.1Hz, achieving structural lightweight while meeting the modal performance matching requirements.

4.2. Sample Data Acquisition

To mitigate the computational burden and high costs caused by simulations, the proxy model construction approach is commonly adopted. The optimal Latin hypercube experimental design method generates sample points with superior scalability and balance. While this method enables more comprehensive distribution of sample points across the entire design space, it has the drawback of requiring longer computation time. Based on the design range of the design variables, a total of 30 sample points is generated, as shown in the table.

4.3. Agent Model Construction and Selection

Given the complex nonlinear relationship between the response of battery case lid mass, modal frequencies, and thickness variations across its regions, direct optimization through finite element simulations or experiments would require substantial computational resources. To address this, this study employs an approximate model linking design variables with response objectives, effectively replacing costly numerical simulations while enhancing multi-objective optimization efficiency.

The core principle of the surrogate model involves establishing a mapping relationship between design variables and response values through polynomial function fitting. Each set of design variable samples is imported into the simulation model for computation to obtain response values at each sample point. The variable values and their corresponding response values are then exported to Isight software, where the appropriate surrogate model is selected for analysis and error evaluation.

Error analysis method using 10-fold cross-validation The fitting accuracy of the approximate model is evaluated using the root mean square error (RMSE) and the coefficient of determination (R2), with the corresponding expressions being:

$$R^2 = 1 - \frac{\sum(y_i - \hat{y}_i)^2}{\sum(y_i - \bar{y})^2},$$

Table 7. Optimal Latin Hypercube Sampling

number	x1	x2	x3
1	4.655	3.621	4.931
2	3	3.483	3.552
3	4.931	4.034	3.207
4	3.207	3.552	4.517
5	4.448	4.586	3
6	4.31	3	4.586
7	4.586	4.793	4.31
8	3.828	4.448	3.345
9	3.621	3.207	3.276
10	4.172	3.828	3.138
11	4.517	3.966	3.828
12	3.345	3.897	3.069
13	5	4.172	4.379
14	4.034	3.69	4.448
15	3.552	4.103	4.862
16	4.241	3.138	3.897
17	4.379	4.31	4.793
18	3.276	4.241	4.172
19	3.897	4.862	4.655
20	3.483	3.069	4.034
21	3.69	3.759	3.759
22	3.069	4.517	3.483
23	4.724	3.345	3.414
24	3.966	4.379	4.103
25	4.103	5	3.69
26	3.414	4.931	3.966
27	4.862	3.414	4.241
28	3.138	4.724	4.724
29	4.793	4.655	3.621
30	3.759	3.276	5

$$\mathrm{RMSE} = \sqrt{\frac{1}{n}\sum(y_i - \hat{y}_i)^2}$$

in the formula,y_I represents the response value of the i−th sample,while the average denotes the mean response value across all sample points. $\bar{y}$ yı ıs the calculated value for the ı − th sample $\widetilde{\text{poınt}}$, and p denotes the total number of samples.

A lower RMSE and higher R2 value indicate better model performance, with RMSE <0.1 and R2> 0.9 typically meeting accuracy requirements.

(1) RSM proxy model

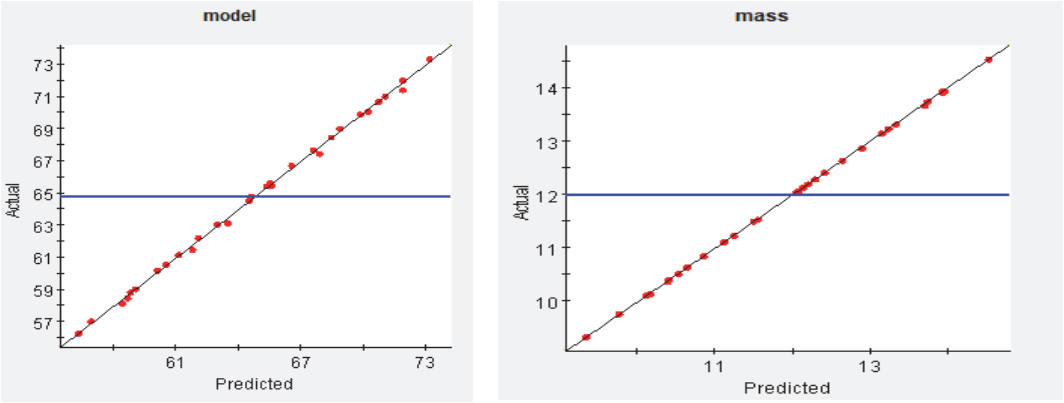


Figure 8. RSM agent model fitting

The RSM surrogate model demonstrates fitting performance for thickness variations at measurement points x1, x2, and x3 on modal first-order frequency (model) and lid mass (mass). Figure (a) shows the fitting plot of modal first-order frequency (model), with RMSE=0.011 and R^2=0.98. Figure (b) illustrates the fitting plot of lid mass (mass),

showing RMSE=0.005 and R^2=0.99. All operating condition models exhibit excellent fitting accuracy.

(2) Kriging Proxy Model

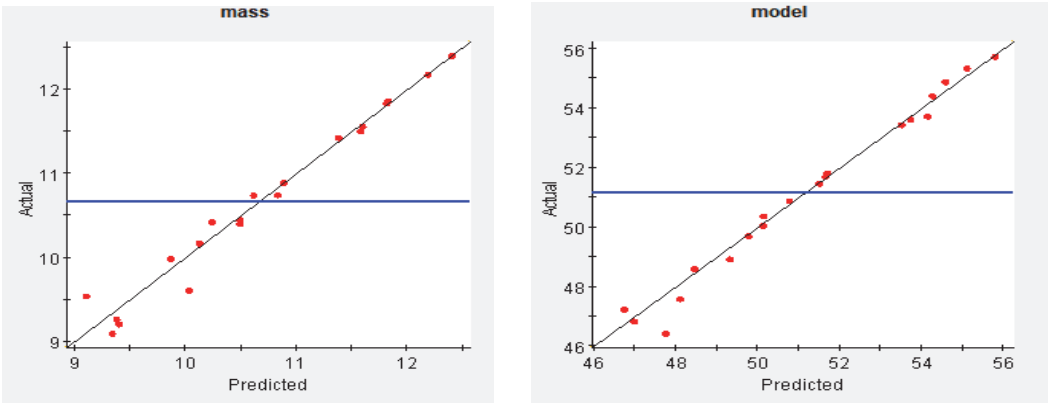


Figure 9. Kriging Proxy Model Fit

The Kriging proxy models fitting performance for thickness variations at measurement points x1, x2, and x3 to the first-order modal frequency (model) and cover mass (mass) is illustrated in the figure. Figure (a) shows the fitting plot of the first-order modal frequency (model), which is

The root mean square error (RMSE) was 0.064, with a coefficient of determination (R2) of 0.95. Figure (b) shows the fitting plot of the upper cover mass (mass), achieving an RMSE of 0.041 and an R2 of 0.98. All operating condition models met the required fitting accuracy.

(3) RBF Proxy Model

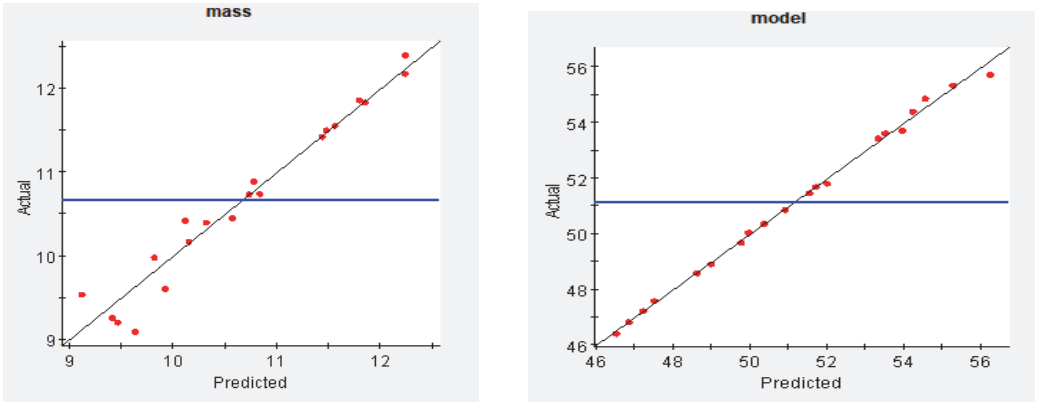


Figure 10. RBF proxy model fitting

The RSM surrogate model demonstrates fitting performance for thickness variations at measurement points x1, x2, and x3 on modal first-order frequency (model) and lid mass (mass). Figure (a) shows the fitting plot of modal first-order frequency (model), with RMSE=0.051 and R^2=0.97. Figure (b) illustrates the fitting plot of lid mass (mass), showing RMSE=0.017 and R^2=0.98. All operating condition models exhibit high fitting accuracy.

Among the three surrogate models, the RSM model outperformed the RBF and Kriging models in both root mean square error (RMSE) and coefficient of determination (R^2), demonstrating its superior fitting accuracy. This indicates that RSM is the more accurate model for subsequent optimization.

4.4. Optimize and Analyze Results

To solve the multi-objective optimization problem of upper cover thickness zoning, the second-generation Non-Dominating Sorting Genetic Algorithm (NSGA-II) was employed. Compared with other multi-objective optimization algorithms, NSGA-II demonstrates faster execution speed and superior solution convergence. The NSGA-II algorithm was configured with 60 individuals, 80 iterations, and a crossover probability of 0.9.

After 4,800 iterations, a total of 712 feasible Pareto solutions were obtained through optimization. The optimized Pareto optimal solutions are listed in the table, with solution 4 (numbered 4) being the best result achieved during iteration 2,749. By substituting the design variables corresponding to this optimal solution into the finite element simulation model, we calculated various responses. The optimized values were then validated through simulation experiments, yielding multi-objective optimization results for roof thickness zoning based on the surrogate model.

Table 8. Pareto optimal solution set

	x1	x2	x3	mass	model
1	3.934644	3.000375	3.000660	11.232926	63.439
2	3.934840	3.000095	3.000120	11.233137	63.441
3	3.934882	3.000000	3.000108	11.233208	63.441
4	3.934664	3.000005	3.000003	11.232658	63.439

(1) Static strength simulation verification and optimization results

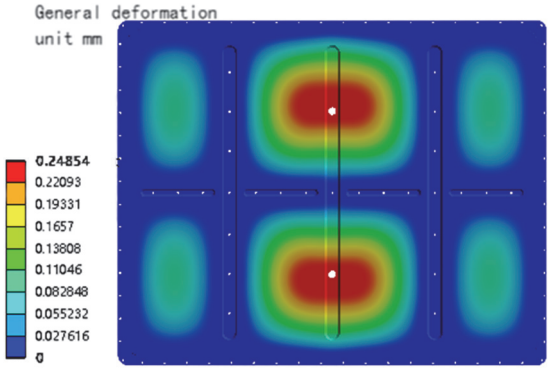


Figure 11. Static strength simulation of bumpy road

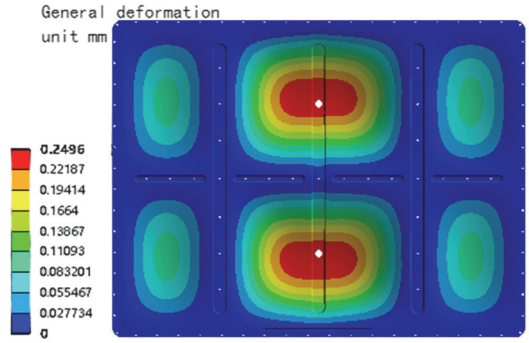


Figure 12. Static strength simulation of bumpy road

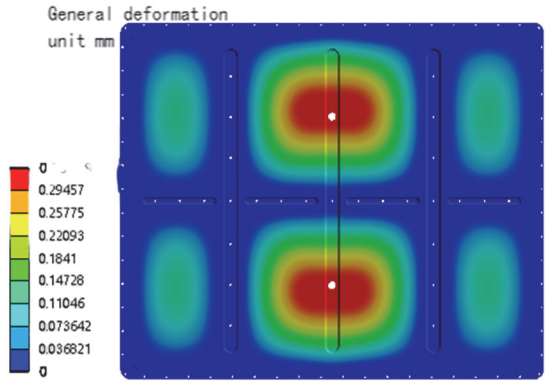


Figure 13. Static strength simulation of emergency braking on bumpy road

(2) Modal simulation verification and optimization results

The optimized simulation results are compared with those from multi-objective optimization to further validate the accuracy and fitting precision of the combined agent model, as shown in the table. Analysis shows that all errors are within 1%, indicating high precision of the agent model and reliable multi-objective optimization.

Table 9. Modal Simulation Comparison

modality /Hz	alufer	postoptimality
first order	63.50	63.68
second order	67.81	66.67
tervalence	75.44	92.14
4th order	77.41	93.24
5th order	85.51	108.84
Sixth order	85.54	108.98

The comparison demonstrates significant lightweight optimization effects. When targeting the first-order modal frequency of aluminum alloy material covers, both the first-order modal frequency and static performance have improved to meet operational requirements. The structural components of aluminum alloy materials show a 1.99kg reduction in mass (15% mass reduction) within the error range of their modal frequency below 0.1Hz, demonstrating effective lightweighting and feasibility. The vehicles overall range is expected to increase by approximately 0. in the 8km NEDC test cycle, the non-flame-retardant version (30% CF/PA66) demonstrates a 25%-35% reduction in top cover production costs and a 40% shorter production cycle. The materials properties enable integrated sealing strips, eliminating the need for separate structural designs and installation processes. This indicates the feasibility of optimized applications in battery pack enclosures once the materials flame-retardant technology matures and costs become manageable.

5. Conclusion

This study establishes a multi-objective optimization design method for composite battery box lids using the NSGA-II algorithm. By applying the equivalent stiffness substitution theory, the 2mm aluminum alloy lid is converted into a 4mm 30% CF/PA66 composite structure. Through collaborative optimization using RSM surrogate models and NSGA-II algorithm, the design achieves a 1.99kg weight reduction (15% weight saving) while maintaining modal error below 0.1Hz (optimized first-order mode 63.68Hz vs aluminum alloy 63.50Hz). Static strength analysis shows the optimized structure exhibits maximum displacement of 0.31mm under 4g vibration conditions, representing a 50% reduction compared to aluminum alloy. The sixth-order mode 108.98Hz effectively avoids the high-frequency vibration range of motors (above 150Hz). Key innovations include:

(1) This study pioneers the application of chopped carbon fiber-reinforced nylon (CFR nylon) in battery case lids, effectively resolving modal splitting issues in conventional CFRP laminates through the isotropic properties of 30% CFR/PA66 blends. (2) The design innovatively incorporates the UL94-V0 flame retardancy standard (3mm thickness) as a variable ($x1-x3\in[3,5]$mm), achieving a balance between safety and lightweight performance. (3) A rapid optimization framework based on Response Surface Method (RSM) surrogate models is established, delivering 80% efficiency gains compared to direct simulation calculations.

The key to implementing this scenario lies in improving the flame retardancy of 30% CF/PA66 and reducing costs. Furthermore, by optimizing the battery case design through topology optimization methods, the weight will be further reduced, aiming for a mass reduction of over 20%.

References

[1] Zhang Xiaohu, Meng Yu, Zhang Wei. Current Status and Trends of Carbon Fiber-Reinforced Composite Material Technology [J]. Fiber Composite Materials, 2004,21(1):50-53.

[2] Zhang Wei, Wang Huimin, Li Xue. Impact performance of carbon fiber-reinforced thermoplastic composites in automotive crash beams. Journal of Composite Materials, 2021,38 (5):1350-1358.

[3] Liu Yong, Chen Li, Jiao Wei, et al. Advances in the Forming Process of Thermoplastic Composites and Their Applications

in Aerospace Engineering [J]. Materials Engineering, 2020, 48 (9): 62-72.

[4] Jia Mingyin, Xue Ping, Sun Anyuan. Recycling and Reuse Technology of Long Fiber-Reinforced Thermoplastic Composites [J]. Engineering Plastics Applications, 2019,47(1): 146-150.

[5] Zhou Xiaodong, Dai Zengying, Dai Gance. Performance Study of Long Carbon Fiber-Reinforced Nylon 66 Composite [J]. Plastic Industry, 2018,46(3):88-91.

[6] GB38031-2025 Safety Requirements for Power Batteries for Electric Vehicles [S].

[7] Morgan A B,Wilkie C A. Flame Retardant Polymer Nanocomposites[M]. John Wiley&Sons,2007.

[8] Markforged Technical White Paper. Onyx FR Material Datasheet [R]. 2024.

[9] Qu Rihua, Wang Liyan, Guan Chong, et al. Thermal Properties of Carbon Fiber-Reinforced Nylon 66 Composites. [J]. Plastic, 2020,49(06):45-49.

[10] Chen Xiaokai, Li Mengqiang, Li Shufeng, Jin Jianguo, Zhang Chuang. Design optimization of multi - material battery enclosure for electric vehicle(M). Lecture Notes in Electrical Engineering, 2019:853-864.

[11] Ma Qi-hua, Dong Fan, Qin Xiao-yu, Ma Qi-hua, Dong Fan, Qin Xiao-yu, et al. Parallel optimization of design and manufacturing—Carbon fiber battery pack for electric vehicles[J]. Mechanics of Advanced Materials and Structures, 2024, 31(10): 2289-2306.

[12] Zhang Qi, Xia Lidong, Li Yuan, et al. Preparation and Properties of High-Performance Carbon Fiber-Reinforced Nylon 10T Composite Materials. Engineering Plastics Applications, 2022,50(05):44-49.

[13] Guo Yongqi, Huang Xiaozheng, Wang Shuai, et al. Development of Carbon Fiber Engine Hood Based on the Principle of Equivalent Stiffness [J]. Automotive Practical Technology, 2017(19):100-103.

[14] Wang Zhenyu, Chen Xiaofeng. Study on the Design Coefficient α for Stiffness Lightweighting of Automotive Components [J]. Journal of Mechanical Engineering, 2022,58 (14): 89-97.

[15] Ministry of Industry and Information Technology of the Peoples Republic of China, State Administration for Market Regulation. Safety requirements for power batteries for electric vehicles: GB 38031-2020[S]. Beijing: China Standard Press, 2020.

[16] Qin Yuying, Cao Junjie. Modal Analysis and Optimization Design of New Energy Power Battery Pack [J]. Power Supply Technology, 2023,47(8):1060-1063.

[17] Wang Kang, Cao Yongsheng, He Qicai, et al. Lightweight Design of White Body Structure Based on Multi-Objective Optimization [J]. Times Automotive, 2023, (22):151-154.

[18] Lin Tianhao, Xu Congchang, Lin Qiquan, et al. Multi-objective optimization of bending forming of 7003-T4 aluminum alloy anti-collision crossbeam using response surface and neural network models [J]. Journal of Plasticity Engineering, 2019, 26 (6): 67-75.

[19] Ruan Zhixin, Chen Chao, Zhan Teng, et al. Multi-objective Optimization of Automotive Seat Performance Using a Combined Agent Model [J]. Mechanical Design, 2024,41(11): 136-143.